Design Optimization for Additive Manufacturing of a 1U CubeSat's Mechanical System

Sofia Lima Carvalho
sofia.carvalho@tecnico.ulisboa.pt

Instituto Superior Técnico, Universidade de Lisboa, Portugal

November 2019

Abstract

Additive manufacturing (AM) is an emerging manufacturing process that is transforming the aerospace industry by creating lighter, stronger and more complex components which were difficult or impossible to fabricate by traditional methods. Continuous development of design optimization tools which estimate the optimal material distribution for a given problem, such as topology optimization (TO), has fostered the production of parts by AM. The combination of AM with TO is beneficial for the aerospace industry as it presents an opportunity for weight and cost saving, while taking full advantage of both technologies. The purpose of this master's dissertation is to develop and optimize a 1U CubeSat Mechanical Subsystem for further production by AM. The procedure adopted for the design of CubeSat began with the determination of project requirements, based on the CubeSat Design Specifications, the P-POD container and the Vega launcher. The structure was optimized and a finite element analysis was carried out to verify if the CubeSat is able to sustain the linear static loads during launch. Following the production of the optimized component, experimental tests were performed to validate the design and computer analysis. The optimized structure presents considerable weight reduction as well as a decrease in the number of components required.

Keywords: CubeSat, Additive Manufacturing, Topology Optimization, Finite Element Method, Aerospace Industry

1. Introduction

The aerospace industry is continuously seeking for innovation and technological progress to efficiently address not only the major challenges of producing high performance products but also the society's yearning for innovation. Consequently, the industry's need for complex and optimized structures led to the introduction of AM in the aerospace sector [1].

In recent years, AM has gained increased attention due to the several advantages it offers, such as: production of components with complex geometries, design freedom, customization, reduction of waste and tooling, among others [2]. One of the primary benefits for the aerospace industry is the production of lightweight parts since the reduction of the overall weight of an aircraft translates in fuel savings and, consequently, in less costs and emissions.

The fast-growing field of TO is of special interest to the aerospace industry since it enables the creation of components with reduced structure volume, weight and cost. Nevertheless, traditional manufacturing processes frequently fail to achieve the designs that result from TO application and therefore AM, for its design freedom and lack of manufacture constraints, emerges as a particularly suited manufacturing process to take full advantage of TO design. Consequently, the combination of TO as a design method and AM is beneficial for the aerospace industry as it presents an opportunity for weight saving and eventually less manufacture costs.

In the past decades, there has been a growing development of missions based on small satellites which led to the development of the CubeSat concept. The CubeSat program was developed in 1999, as a collaboration between the California Polytechnic State University and Stanford University. Since the launch of the first CubeSat, several government agencies, like the European Space Agency (ESA), the National Aeronautics and Space Administration (NASA) and others, adopted the CubeSat standard and so encouraged the growth of CubeSat-based missions [3]. Despite the intrinsic challenges to CubeSat missions that still need to be addressed, new research and technological advances will continue to drive the space industry to invest in the utilization of CubeSat platforms both for commer-

cial and scientific purposes [4].

This work aims to develop and optimize the $1U$ *CubeSat* mechanical subsystem and to manufacture the first prototype of the structure with AM, with the support of CEiiA.

2. Background

This chapter provides a review of theoretical concepts relevant to this study, being fundamental to create a foundation for the research work carried out in this dissertation.

2.1. Additive Manufacturing

AM, also known as 3D printing, is a "process of joining materials to make objects from 3D model data, usually layer upon layer, as opposed to subtractive manufacturing methodologies", as defined by the American Society for Testing and Materials (ASTM). AM processes may be categorized with respect to the material feedstock, heat source,the deposition technique, amongst others [5]. Currently, metals are one of the most commonly used materials in AM. Metal Additive Manufacturing (MAM) is an attractive alternative to traditional processes as it presents numerous benefits for a wide range of applications and can be used in several markets to solve different problems in a rapid and sustainable way. Some of the main advantages of MAM include: production of components with complex geometries and shapes, reduction of the number of parts in a product, manufacture of lightweight parts, customization, and so forth. Powder Bed Fusion (PBF) is one of the most relevant MAM processes and one of its techniques, the Selective Laser Melting (SLM), will be discussed in this work. SLM is a PBF technology in which a high powered laser is used to melt metallic powders to build up the part, in agreement with the information provided by a CAD file [5].

2.2. Structural Analysis

The Finite Element Method (FEM) is a numerical approach used to determine the approximate solution of differential equations that describe a physical phenomenon on a defined domain [6]. The main goal of FEM is the discretization of a continuous system into finite elements, connected by nodes, generating the finite element mesh. The calculation is performed at the nodes, which are coordinate locations in space where the degrees of freedom (DOF) are defined. The number of DOF depends on the type of element and the type of analysis [7].

2.2.1 Linear Static Analysis

For the case of static analysis, the force must show no variation with respect to time, and equilibrium conditions must be achieved, with the summation of all external forces and moments being equal to the internal reaction forces and moments. The basic finite element equation to be solved for structures experiencing static loads can be defined as:

$$[K] \cdot \{u\} = \{F\} \tag{1}$$

where K is the global stiffness matrix of the structure, u is the displacement vector and F is the external forces vector applied to the structure. This equation expresses the equilibrium between external and internal forces [7].

2.3. Topology Optimization

The general TO problem can be written in mathematical form as:

$$\begin{aligned} \text{Minimize} \quad & F(\mathbf{u}(\rho), \rho) = \int_{\Omega} f(\mathbf{u}(\rho), \rho) dV \\ \text{w.r.t.} \quad & \rho\,, \qquad (2) \\ \text{subject to} \quad & G_0(\rho) = \int_{\Omega} \rho(x) dV - V_0 \leq 0 \\ & G_j(\mathbf{u}(\rho), \rho) \leq 0, j = 1, ..., m \qquad (3) \\ & \rho(\mathbf{x}) = 0 \; or \; 1 \forall \; \mathbf{x} \in \Omega\,, \end{aligned}$$

where F is the objective function to be minimized, Ω is the design domain, G_0 is a volume constraint, G_j are other possible constraints, $\rho(x)$ is the material distribution, f is a local function and u is the state field which satisfies the state equation. The optimization problem consists in finding the material distribution, $\rho(x)$, that minimizes the objective function F, subject to the a volume constraint G_0 and m other possible constraints G_j [8, 9].

The method addressed in this dissertation is a density-based method called Solid Isotropic Material with Penalization (SIMP). The SIMP method keeps a fixed finite element discretization where each finite element is associated with a density distribution $\rho(x)$ whose value lies between zero (void) and one (solid) [9]. In the SIMP approach the relation between the density design variable and the material property is given by:

$$E_e(\rho(x)) = \rho(x)^p \cdot E_0 \tag{4}$$

where p is the penalization parameter, E_0 is the elastic modulus of solid material and the $E_e(\rho(x))$ is the element elastic modulus [8]. The penalization parameter p is imposed to every element's stiffness as follows:

$$K_e = \rho(x)^p \cdot K_0 \tag{5}$$

where where K_e is the stiffness of the element, p the penalization parameter and K_0 is the stiffness of the material [10]. According to [10],the lowest allowable penalization parameter p for a three-dimensional analysis is three and can be defined as:

$$p \geq max\{15\frac{1-v^0}{7-5v^0}, \frac{3}{2}\frac{1-v^0}{1-2v^0}\} \quad (6)$$

where v^0 is the Poisson ratio of the material.

2.4. Small Satellites

In the past decades, there has been a growing development of missions based on small satellites which led to the development of the CubeSat concept. The CubeSat program was developed in 1999, as a collaboration between Prof. Jordi Puig-Suari, from California Polytechnic State University, and Prof. Bob Twiggs, from Stanford University. As stated in the CubeSat Design Specification (CDS), "a CubeSat is a 10 cm cube with a mass of up to 1.33 kg". They are measured in units $U = 10 \times 10 \times 10\ cm^3$ and this form factor ranges from 1U up to 12U, although new configurations are under development [11]. CubeSats are progressively transitioning from educational tools and technology demonstrating platforms to real science or commercial missions, creating the opportunity for missions with high scientific return or revenue and with less costs than traditional missions [12]. The Poly Picosatellite Orbital Deployer (P-POD), developed by the California Polytechnic State University, was selected as the CubeSat's container. The P-POD is a standard deployment system whose primary goal is to provide a common interface between CubeSat and launch vehicle [13]. The Vega launch system was adopted as the CubeSat's launcher. Vega was developed by ESA and the Italian Space Agency, with the goal of launching small satellites for scientific and Earth observation missions [14].

2.4.1 General System Architecture

A CubeSat can be divided into three segments: the ground segment, the launch segment and the space segment, according to Figure 1. First, the ground segment comprises the communication between the vehicle and the ground station. Secondly, the launch segment includes the launch vehicle responsible for the transportation of the spacecraft to orbit. Lastly, the space segment can be split into two modules: the payload and service module. The payload module covers all the equipment specific for the mission and the service module combines the subsystems necessary for its operation. The service module consists of 6 subsystems: the Mechanical Subsystem and Structures (MSS), the Thermal Control Subsystem (TCS), the Electrical Power subsystem (EPS), the Attitude Determination and Control subsystem (ADCS), the Command and Data Handling subsystem (CDH) and the Telemetry, Tracking and Control subsystem (TTC) [15].

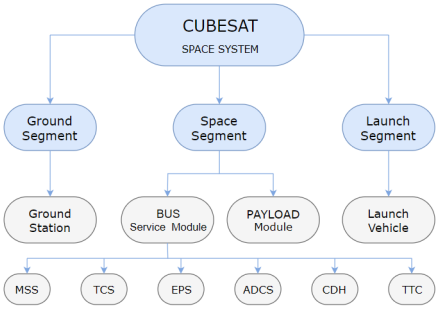

Figure 1: Architecture Diagram of the CubeSat System [15]

3. Implementation

The challenge of this work is to develop and optimize the 1U CubeSat mechanical subsystem to be further manufactured by AM and used in future space missions. When designing a new satellite structure various regulations must be considered in order to guarantee that the final design will fulfill all of its objectives. The 1U CubeSat project requirements were divided into Mission requirements and Design requirements, set in accordance with the CubeSat Design Specifications [11].

4. Results

Initially, an analysis of the current 1U CubeSat structure solution proposed by CEiiA was performed. The developed structure is composed of an Al7075 aluminum alloy, weighs approximately 85g and consists of six components: four ribs and two side frames, as depicted in Figure 2.

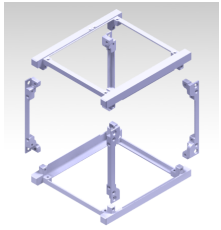

Figure 2: Current 1U CubeSat Structure Solution

The structure developed by CEiiA was designed to be manufactured by conventional methods. However, the new solution is to be manufactured by AM, with the ultimate goal of minimizing the weight or the number of parts through an innovative assembly configuration. Hence, the new structure was divided into two L-shaped components and has incorporated drawers to hold the electronic components inside the CubeSat, as shown in the Figure 3. After the integration of all the service module subsystems and the design of the mechanical subsystem, the preliminary design of the 1*U CubeSat* structure was concluded.

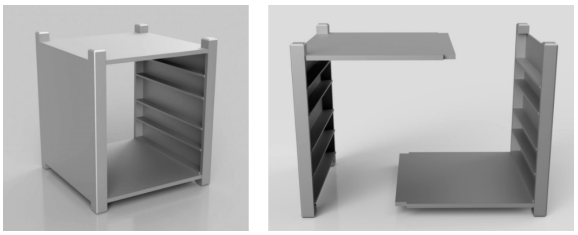

Figure 3: Assembly of the proposed 1U CubeSat

4.1. 1U CubeSat Topology Optimization

The *Autodesk Fusion* 360 software was used to to perform the TO of the new $1U$ *CubeSat* structure. Considering that *Fusion* 360 does not allow the TO of assemblies, the two L-shaped components were united in *CATiA* so as to form a single solid capable of being subjected to simulation. The previously defined geometry underwent through some changes and the proposed new model weighs 0.202kg, as portrayed in Figure 4.

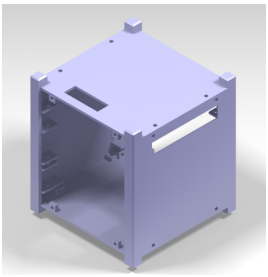

Figure 4: 1U CubeSat model before TO

The first step of the TO process was to define the material under study. Thereby taking into account the design requirements mentioned earlier, Aluminum $AlSi10Mg$ was the material chosen to produce the parts. The mechanical properties of the powder, printed at 0^{o}, were introduced into the material library of *Fusion* 360.

Secondly, the loads and point masses were specified. The structural subsystem must resist the longitudinal and lateral loads imposed by the VEGA launcher during all the phases of ascension. As stated in the Announcement of Opportunity on a Vega Flight [16], the CubeSat will experience the highest accelerations during the launch sequence: 14.5g in compression and 10.5g in tension, both in the y axis; 3g in the x and z axis, both in compression and tension, as shown in Figure 5. Additionally, it was essential to calculate the positions of the center of gravity of each electronic component and its attachments to the structure. Thus, considering the physical characteristics of each electronic component the respective equivalent point masses were assigned within the model.

In the third place, the constraints must be applied to the structure. The CubeSat will be simply supported since it is not fixed inside the P-POD and solely its rails touch the deployer. Accordingly, for each gravity load, constraints were applied on surfaces opposite to the movement, blocking it in that direction, and the rails vertices were constrained in the other two directions to avoid infinite displacement of the part. Furthermore, as the simulation will remove material from the model, it is required to ensure that material will remain present around critical areas of the model. In this way, the areas of material to be preserved in the structure were determined. With respect to $1U$ *CubeSat*, the critical zones that must be preserved are the rails, the edges, the holes in the drawers to secure the electronic components and the holes in the CubeSat walls to accommodate the solar panels.

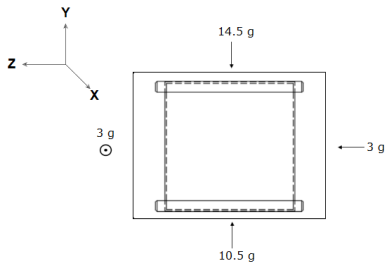

Figure 5: Loads acting on the CubeSat inside the VEGA launcher

Moreover, the mesh element type and size were determined. The creation of the mesh is essential to the finite element analysis because the quality of the mesh directly influences the quality of the results generated. For this model, parabolic tetrahedral elements with curved edges were chosen, composed of four triangular faces and six edges each. Subsequently, the smallest possible size was assigned to the mesh as the simulation was performed in the cloud, which allowed to greatly reduce the computation time and simultaneously increase the mesh quality.

Eventually, the target mass was set to 50% and results were obtained in terms of load path criticality. The load path criticality is a discrete variable ranging from 0 to 1, with 1 representing red regions in the model that are critical in resisting the applied load and 0 representing blue regions that are not critical in resisting the applied load. The load path criticality results were reviewed for all the gravity loads mentioned above. By way of example, both the first and final results for the 14.5 g gravity load are illustrated in Figures 6 and 7, respectively.

As evidenced in the Figures 6 and 7, the first result presents the original model with 0.202 kg whereas the last result shows the new developed

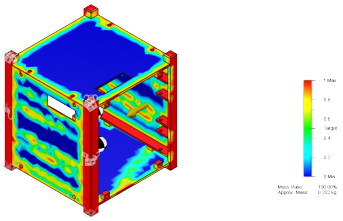

Figure 6: First result of the TO

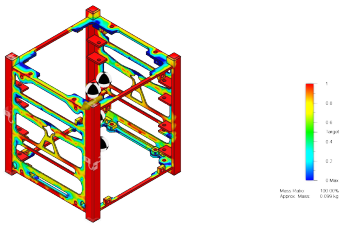

Figure 7: Last result of the TO

model with 0.099 kg, thereby achieving the goal of weight reduction through TO. Once the result depicted in Figure 7 is accepted, the mesh generated will be used as a template for making modifications to the original geometry. In fact, the mesh is exported to the design workspace and is automatically superimposed on the original model design, as illustrated in Figure 8. Then, closed sketch objects are created around the material to be removed and after cut out to leave only the required geometry. Lastly, the final model developed from the last result of the TO is presented in Figure 9.

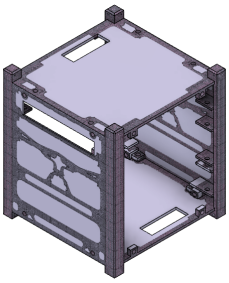

Figure 8: Mesh superimposed on the original model

Comparing the new solution with the structure initially proposed by CEiiA, which weighs 85g, a mass increase of 16% is noticed. However, considering that the drawers incorporated in the new solution replace the rods used for mounting the nanodocks, according to the PC/104 staking method, and these in turn weigh 20g in total, this means that actually there is a mass reduction achieved with the new solution. Bearing in mind that the structure proposed by CEiiA together with the rods would approximately weigh 105g and that the new developed solution, which integrates the drawers that replace these rods, weighs 99g, there is actually a 6% mass reduction. Besides, with the new solution, the number of components has decreased from six to two. Consequently, it can be concluded that the new solution accomplishes both weight and component reduction of 6.0% and 66.7%, respectively. In conclusion, with TO was possible to achieve a lighter structure and with fewer assembly components, which is of the utmost importance in the space industry, where there is a growing interest in optimizing structures in terms of weight [17].

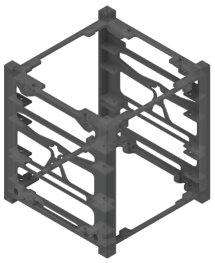

Figure 9: Model developed on *Fusion* 360

4.2. 1U CubeSat Structural Analysis

A static stress analysis is required to verify if the final model meets the design requirements. For this reason, to validate the model obtained it is indispensable to simulate its behavior when the critical loads are applied, in order to verify that no failures occur during its use. Accordingly, *Autodesk Fusion* 360 software was used to perform the static stress study.

The first step of the static stress analysis was to define Aluminum $AlSi10Mg$ as the material under study, introducing the mechanical properties of the powder into the material library of *Fusion* 360 .

Next, the forces and respective constraints were applied to the $1U$ *CubeSat* structure. Besides the six gravity loads formerly described in the Figure 5, a seventh simulation was performed in which the gravity load vector was defined as the sum of $14.5g$ on the y axis, $3g$ on the x axis and $3g$ on the z axis. This last simulation represents the case that will probably be more critical for the $1U$ *CubeSat* structure since the satellite is subjected to the greatest gravity load vector possible [16].

Prior to the simulation it was necessary to determine the mesh parameters. As already discussed the elements used in *Fusion* 360 are parabolic tetrahedral elements with curved edges and it is essential to estimate their most suitable size for the $1U$ *CubeSat* model. From this perspective, a mesh convergence study was conducted to ensure the accuracy of simulation results. The entire CubeSat structure was used for the convergence study and

the 14.5 g gravity load was chosen. In order to find the dimensions of the mesh for which the displacement and stress values converge, various element sizes were considered from $0.5t$ to $1.5t$, where $t = 1\ mm$ is the minimum model thickness. When performing the mesh convergence study, the displacement and stress comparison were based on a consistent vertex of the geometry since the mesh may be different for each iteration. The results of the mesh convergence study for both the displacement and stress are shown in Figures 10 and 11. Eventually, the displacement and stress results level off when the mesh element number is around 1500000, corresponding to $0.5t$. Ultimately, further mesh density increase would have a diminishing effect on the results and a higher computational time, so a mesh with parabolic tetrahedral elements with 0.5 mm side was created.

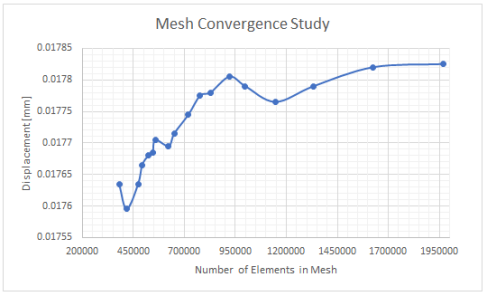

Figure 10: Mesh Convergence Study - Displacement

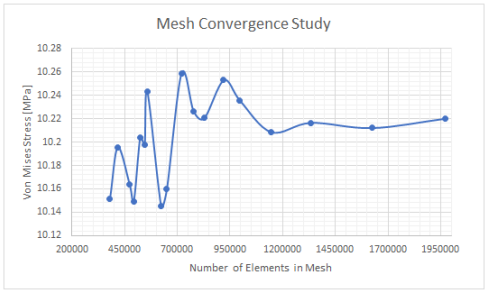

Figure 11: Mesh Convergence Study - Von Mises Stress

After all the conditions were established, the simulation was solved and results in terms of stress, displacement and safety factor were obtained.

4.2.1 Stress Distribution

In *Fusion* 360, the solver outputs six stress tensors and three combined stress results, known as Von Mises Stress, 1^{st} and 3^{rd} Principal Stresses. Usually, the multidirectional stress tensors are combined into an equivalent stress magnitude, the Von Mises stress, σ_v. The Von Mises stress can be described by the following equation:

$$\sigma_v = \left(\frac{(\sigma_{xx} - \sigma_{yy})^2 + (\sigma_{yy} - \sigma_{zz})^2 + (\sigma_{zz} - \sigma_{xx})^2}{2} = +3 \cdot (\sigma_{xy}^2 + \sigma_{yz}^2 + \sigma_{zx}^2) \right)^{0.5} \tag{7}$$

This equation is applicable to isotropic materials, which have the same modulus of elasticity E and Poisson's ratio v for loads applied in any direction. In order to predict failure in the $1U$ *CubeSat* structure the Von Mises stress will be compared to the yield strength of the Aluminum $AlSi10Mg$.

Following the simulation of the seven gravity loads aforementioned, it was confirmed that the seventh simulation is the most critical scenario for the $1U$ *CubeSat* structure since it presents the higher Maximum Von Mises Stress. Thus, the stress results of the seventh simulation are portrayed in Figure 12.

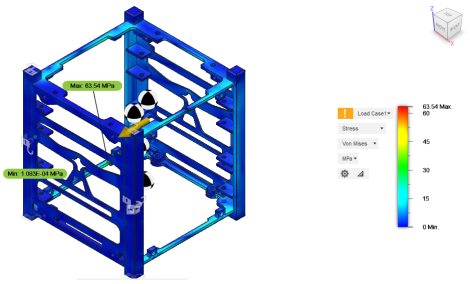

Figure 12: Stress distribution

As evidenced in Figure 12, the model will reach a maximum Von Mises stress of approximately 63.540 MPa, which is very localized and well above the average stress. In view of the fact that $AlSi10Mg$ has an average yield strength of 190 MPa and a ultimate tensile strength of 330 MPa [1], both the average and maximum stress, for all seven simulations, are well below the yield strength of the material. Hence, it can be concluded through the analysis that the stresses to which the component may be subjected will not cause material plastic deformation or even fracture.

4.2.2 Displacement

In addition, it is important to investigate the results in terms of the displacement of the $1U$ *CubeSat* structure from its original position. Although the previous results do not predict the existence of plastic deformation, it is possible that there may be

[1] Information given by CEiiA's supplier Trumpf

a small elastic deformation of the material, recoverable after the removal of the gravity loads. Regarding the model displacement results, the seventh simulation is illustrated in Figure 13 .

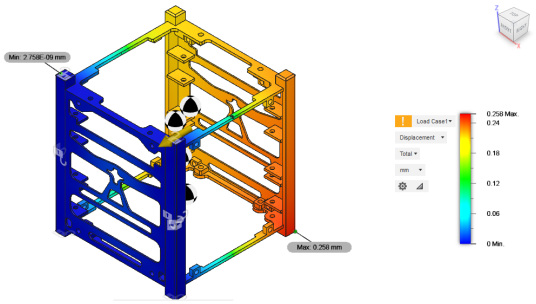

Figure 13: Displacement

Analyzing Figure 13, it is clear that when the component is subjected to the greatest gravity load vector possible, it may suffer a maximum displacement of approximately 2.580×10^{-1} mm, relative to its initial position. As would be expected, this displacement will occur in the side wall where the loads are applied and the farthest from its fixed area. On the contrary, moving towards the wall where the constraints are applied, the displacement decreases until it reaches zero. This gradual reduction in displacement, from the surface where the forces are applied to the surface where the constraints are applied, is verified for all the other simulations. Beyond this, it may be concluded that the maximum displacements computed can be considered negligible since there is no occurrence of plastic deformation and the structure shows no permanent deformation even when the expected maximum forces are applied.

4.2.3 Safety Factor

The safety factor describes how much stronger a system is than it is required for a predefined load, thus assessing how suitable a design is for its intended application. In *Autodesk Fusion* 360, the safety factor is calculated as the ratio of the material yield strength and the Von Mises equivalent stress, specifying whether the design is likely to bend or break when submitted to the applied loads:

$$SF = \frac{Material\ Yield\ Strength}{Von\ Mises\ Stress} \tag{8}$$

The safety factor results are extremely relevant because, in the real world, all aspects of the design present some degree of uncertainty and therefore a factor of safety is imperative. In this manner, the minimum safety factor results for the seventh simulation represented in Figure 14.

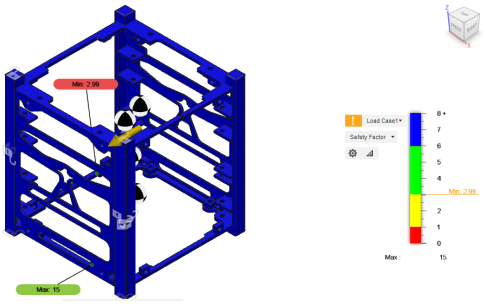

Figure 14: Safety factor

Generally, the greater the risk of component failure the greater the safety factor should be. In the present case, the highest risk that could result from the 1*U CubeSat* structure failure would be to jeopardize the mission objectives. Taking into account that NASA and the aerospace industry have strict guidelines for design factors, the choice of safety factor for this project was based on their standards [18]. However, considering that several assumptions were made throughout the simulations, the selection of the safety factor was even more conservative. In this way, the minimum safety factor for the 1*U CubeSat* structure was defined as 2.0. Examining the Figure 14, it is clear that the 1*U CubeSat* structure has an average safety factor higher than 6, which is more than necessary to ensure that this component resists the predefined critical loads. Nonetheless, it should be noted that the lowest safety factor found was 2.99. As expected, the lowest safety factor was obtained in a small area, identified in the Figure 14, coincident with the region in which the highest accumulated stresses were observed in the Figure 12. Overall, the results obtained for the safety factor are considered acceptable, since practically the whole volume of the 1*U CubeSat* mechanical subsystem has a safety factor greater than 6, and even the areas below this value have a safety factor bigger than 2 and which allows them to handle loads 2.99 times higher than the predefined critical loads. Finally, after verifying all the results provided by the finite element analysis performed, it can be concluded that the 1*U CubeSat* mechanical subsystem is validated in terms of stress,displacement and safety factor.

4.3. Manufacturing Process Simulation

AM process simulation is an innovative and necessary tool to fully exploit the potential of AM since errors associated with this manufacturing technology can be predicted and further reduced.

After the structure has been validated, a simulation of the manufacturing process was performed to predict the outcomes of printing the 1*U CubeSat* structure using SLM. *Amphyon* was the software

selected to simulate the manufacturing process.

In order to simulate the manufacturing process it was first necessary to select $AlSi10Mg$ as the material and specify its properties in Amphyon's workspace. Likewise, the $TruPrint$ 3000 machine was selected to produce the $1U$ $CubeSat$ structure and its parameters were defined in Amphyon's workspace. Next, the assessment tool of *Amphyon* was used to determine the ideal orientation of the 1U CubeSat structure within the Trueprint 3000 build-chamber and two optimal orientations were generated, as represented in Figure 15.

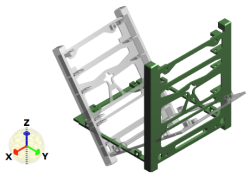

Figure 15: Optimal orientation results with Amphyon

Afterwards, the *Amphyon* support generation tool was used to create the support structures that are adapted to the specific needs of 1U CubeSat model. Subsequently, the supports were created as shown in Figure 16.

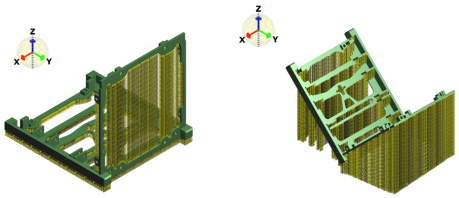

(a) First orientation (b) Second orientation

Figure 16: Generated supports in Amphyon

Upon completion of the manufacturing process simulation, displacement and stress results were obtained. The displacement results represent the distance that the component moves in relation to the original geometry at a given point in the manufacturing process. The displacement generated during manufacture is due to internal stresses accumulated in the components, which, in turn, are created by the expansion and contraction of the material due to the large thermal gradients inherent to the process. The largest displacements computed were 2.72 mm and 2.83 mm for the first and second orientation, respectively. By analyzing the results, one can conclude it is still possible to decrease the displacement of the component by, for example, pre-heating the chamber, the manufacturing platform and the metal powder. The stress results provided by *Amphyon* describe the stress experienced by the component after manufacture and which can eventually lead to structure failure. Usually, component failure is associated with the displacement generated by accumulated residual stresses in the component. In general the structure presents stresses below the yield strength of the $AlSi10Mg$ but in some small regions the maximum stress is above yield strength and thus the structure failure is confirmed for both orientations. In order to address this problem and improve the manufacturing process, one solution would be to create more robust and resilient support structures since they would allow an improvement in heat transfer to the manufacturing platform, significantly reducing the stresses caused by thermal gradients. Another suggestion would be to preheat the chamber, work platform and metal powder to reduce the thermal gradients caused by the process, and consequently, the internal stresses.

4.4. Production Process

Tensile tests were performed to characterize the behaviour of the powder material and to verify if the mechanical properties of $AlSi10Mg$ previously assumed are similar to the real values obtained in the experimental tests. In this way, nine specimens were manufactured by Trumpf according to the ASTM Standard E8/E8M-13a [19]. The first batch consisted of four specimens without heat treatment whereas the second batch was composed of five heat treated specimens, both with orientations at 0°, 45° and 90°. The tensile tests were performed according to the ASTM E8M standard on the Instron 3669 machine and an extensometer was used to measure the elongation δ of the specimens. Afterwards, the Elastic modulus, E, the yield strength at 0.2 per cent of elongation, $\sigma_{0.2}$, and the tensile strength, σ_m, were estimated based on the stress-strain curves obtained in Figures 17 and 18.

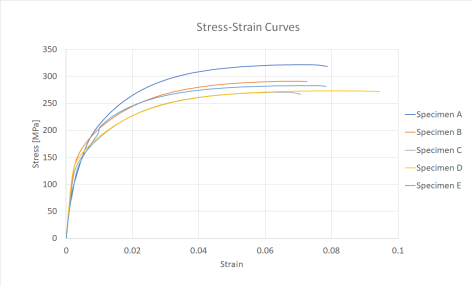

Figure 17: Stress-strain curves for heat treated specimens

The mechanical properties of the $AlSi10Mg$ powder, used in the TO and in the structural analysis to validate the $1U$ $CubeSat$ structure, were defined for powder printed at 0° and without heat treat-

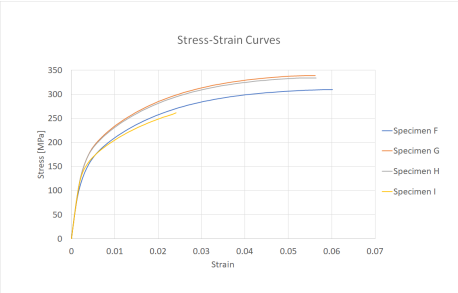

Figure 18: Stress-strain curves for as-fabricated specimens

ment. For this reason, it is relevant to analyze the results obtained for the specimens printed with a 0° orientation and without heat treatment. Table 1 shows the mechanical properties of the powder produced by Trumpf (A), the average of the experimental values obtained for specimens printed at 0° and without heat treatment (B), and the error between these values. Observing the Table 1 it is possible to conclude that the values of the yield and tensile strengths, $\sigma_{0.2}$ and σ_m, are acceptable considering that they present a small error of approximately 2% when compared to the values proposed by Trumpf. On the contrary, the value of the modulus of elasticity E obtained in the tests shows a slightly considerable error of about 7%.

	E [Mpa]	$\sigma_{0.2}$ [Mpa]	σ_m [Mpa]
A	75000	190	330
B	70075.50	186.38	336.84
Error [%]	6.57	1.91	2.07

Table 1: Mechanical properties comparison

In light of this, a static stress analysis was run to verify whether the difference in the mechanical properties would have significant consequences for the stability of the structure of the 1U *CubeSat*. For this purpose, the simulation was again run for the seventh simulation, where all loads are applied to the structure. As can be seen in Figure 19, the change in the mechanical properties of the material only creates slight differences in the displacement and safety factor results. Despite the results presented, it is concluded that the difference in mechanical properties is not sufficient to affect the validity of the simulations previously performed. In conclusion, the finished parts are depicted in Figure 20.

(a) Stress

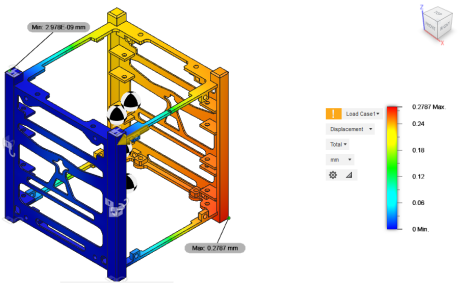

(b) Displacement

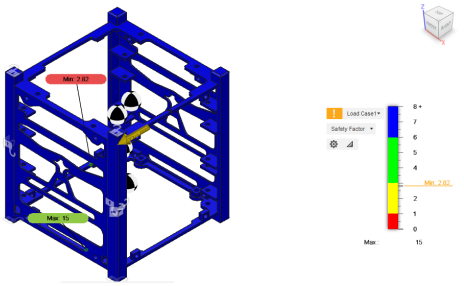

(c) Safety Factor

Figure 19: Static stress analysis with new mechanical properties

5. Conclusions

This dissertation aimed to develop and optimize an original structure for the 1U *CubeSat*, with the ultimate goal of minimizing the weight and the number of parts. Firstly a literature review was conducted on the most important concepts behind the processes that supported this work. Secondly, an investigation of the mission and design requirements was carried out and a preliminary design of the 1U *CubeSat* was accomplished on CATIA. Additionally, a TO was performed and the optimized structure obtained presents both weight and component reduction of 6.0% and 66.7%, respectively. Then, a FEM structural analysis was executed to verify if the CubeSat is able to sustain the launch loads, validating the 1U *CubeSat*. Prior to the production of the structure, a simulation of the manufacturing process was performed to predict the outcomes of printing the 1U *CubeSat* structure using SLM. Finally, a new optimized structure of the 1U *CubeSat* was successfully produced by AM and experimental tests validated the mechanical properties used in the computer analysis, which confirmed the success of the design and the successive steps that led to its production.

Ultimately, further work can be done to improve

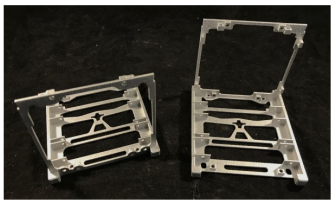

Figure 20: Finished parts

the process of developing, optimizing and producing a 1*U CubeSat* structure. The first step in the future work must be the analysis of the 1*U CubeSat* structure with the real subsystems inside the *CubeSat* as their presence will affect the stiffness of the structure and the design may have to be revaluated. Moreover it is indispensable that transient, random vibrations, and thermal analysis are performed.

Acknowledgements
The author would like to thank to Professor Joana Mendonça, for the immeasurable guidance, motivation and availability throughout the entire project. The author would also like to express her gratitude to Engineers Bruno Rodrigues and Manuel Oliveira for the opportunity to participate in the project and for all the support given at CEiiA.

References

[1] Ian Gibson, David Rosen, and Brent Stucker. *Additive Manufacturing Technologies 3D Printing, Rapid Prototyping and Direct Digital Manufacturing*, chapter 19. Springer-Verlag New York, 2015.

[2] Mohsen Attaran. The rise of 3-D printing: The advantages of additive manufacturing over traditional manufacturing. *Business Horizons*, 60(5):677–688, September 2017.

[3] SpaceWorks. 2019 Nano/Microsatellite Market Forecast 9^{th} Edition, 2019.

[4] Charles L. Gustafson and Siegfried W. Janson. Think big, fly small. In *Pushing the Boundaries of Space*. The Aerospace Corporation, 2014.

[5] William E. Frazier. Metal Additive Manufacturing: A Review. *Journal of Materials Engineering and Performance*, 23(6):1917–1928, 2014.

[6] Jacob Fish and Ted Belytschko. *A First Course in Finite Elements*. John wiley & Sons, 2007.

[7] Daniel Gay and Jacques Gambelin. Practical Aspects of Finite Element Modeling. *Modeling and Dimensioning of Structures*, pages 407–461, 2010.

[8] Ole Sigmund and Kurt Maute. Topology optimization approaches: A comparative review. *Structural and Multidisciplinary Optimization*, 48(6):1031–1055, 2013.

[9] L. Siva Rama Krishna, Natrajan Mahesh, and N. Sateesh. Topology optimization using solid isotropic material with penalization technique for additive manufacturing. In *Materials Today: Proceedings*, 2017.

[10] Joshua D. Deaton and Ramana V. Grandhi. A survey of structural and multidisciplinary continuum topology optimization: Post 2000. *Structural and Multidisciplinary Optimization*, 49(1):1–38, 2014.

[11] Simon Lee, Amy Hutputanasin, Armen Toorian, Wenschel Lan, Riki Munakata, Justin Carnahan, David Pignatelli, and Arash Mehrparvar. CubeSat Design Specification Rev. 13 . *The CubeSat Program, Cal Poly SLO*, 2014.

[12] Armen Poghosyan and Alessandro Golkar. CubeSat evolution: Analyzing CubeSat capabilities for conducting science missions. *Progress in Aerospace Sciences*, 88:59–83, 2017.

[13] R. Nugent, Wenschel Lan, Riki Munakata, Justin Carnahan, and David Pignatelli. Poly Picosatellite Orbital Deployer Mk. III Rev. E User Guide . *The CubeSat Program, Cal Poly SLO*, 2014.

[14] Arianespace. The World's Spaceport. Technical report, Arianespace, 2018.

[15] CEiiA. *N-MACSE Nano Magnetic Attitude & Control System Experiment*, 2019.

[16] Renato Lafranconi. Announcement of opportunity for the launch of multiple light satellites on a vega flight. Technical report, ESA, 2017.

[17] Flaviana Calignano, Diego Manfredi, Elisa Paola Ambrosio, Sara Biamino, Mariangela Lombardi, Eleonora Atzeni, Alessandro Salmi, Paolo Minetola, Luca Iuliano, and Paolo Fino. Overview on additive manufacturing technologies. *Proceedings of the IEEE*, 105(4), 2017.

[18] NASA. Structural Design Requirements And Factors Of Safety For Spaceflight Hardware, 2016.

[19] ASTM International. E8/E8M-13a Standard Test Methods for Tension Testing of Metallic Materials, 2013.